Metallomics

PAPER

View Article Online
View Journal | View Issue

Cite this: *Metallomics*, 2019, **11**, 1900

Low-molecular-mass iron complexes in blood plasma of iron-deficient pigs do not originate directly from nutrient iron†

Nathaniel Dziuba,[a] Joanne Hardy[b] and Paul A. Lindahl *[ac]

Nutrient iron entering the blood binds transferrin (TFN)[d], which delivers iron to cells in the body. In healthy individuals, ~30% of TFN is iron-bound while the remainder is unbound (apo-TFN). TFN saturates the plasma of individuals with iron-overload diseases such as hereditary hemochromatosis, prompting release of a poorly-defined low-molecular-mass (LMM) iron species called non-transferrin-bound iron (NTBI). An experiment was devised to directly detect NTBI in plasma of iron-deficient pigs and to assess the role of the liver which is known to bind NTBI. Catheters were surgically installed in the portal vein (PV) and either the caudal vena cava or the cranial vena cava. After the animals recovered, ^{57}Fe II ascorbate was injected into the stomach *via* a feeding tube. Blood was removed through the catheters before and after injection; plasma became ^{57}Fe-enriched after injection. ^{57}Fe-enriched plasma was passed through a 10 kDa cutoff membrane and the flow-through solution (FTS) was subjected to size-exclusion liquid chromatography (LC). The eluent flowed into an ICP-MS where ^{56}Fe and ^{57}Fe were detected. Low-intensity iron peaks with masses of 400–1600 Da were observed, but none became enriched in ^{57}Fe after injection. Rather, the injected ^{57}Fe bound to apo-TFN. Viewed naively, this implies that nutrient-derived ^{57}Fe in healthy mammals passes from the intestines to apo-TFN without first entering the blood as a LMM intermediate. In this case, nutrient iron exported from intestinal enterocytes of healthy individuals may quickly bind apo-TFN such that LMM iron species do not accumulate in blood plasma. Some ^{57}Fe from the FTS may have adsorbed onto the column. In any event, the LMM iron species in plasma that eluted from the column must have originated from iron stored within the body, perhaps in macrophages – not directly from nutrient iron absorption. The liver absorbed and released LMM iron species, but the effect was modest, consistent with its role as a dynamic iron buffer. Passage through the liver also altered the distribution of different forms of TFN present in the PV.

Received 9th June 2019,
Accepted 23rd August 2019

DOI: 10.1039/c9mt00152b

rsc.li/metallomics

Significance to metallomics

The blood of individuals with iron-overload diseases contain a toxic, labile, low-molecular-mass iron complex called NTBI that enters the blood when too much nutrient iron is absorbed. The chemical composition of NTBI remains undetermined despite intense efforts. NTBI is toxic because it readily binds the liver and other organs. Here, a novel experiment was performed to bypass the effect of the liver and detect NTBI using liquid chromatography. Several low-mass iron complexes were detected, but none originated from nutrients in the stomach. Rather, they appear to originate from iron stores in the body, perhaps from macrophages.

Introduction

The majority of iron in humans is found in erythrocytes as iron-containing heme centers, but this transition metal is also essential for many metalloenzymes and processes as diverse as mitochondrial energetics and DNA replication. Approximately 1 mg of iron enters the body daily through the diet, whereas ~25 mg of iron is recycled.[1] Circulating erythrocytes have a 120 day lifespan after which they are degraded by Kuppfer macrophages in the liver and red pulp macrophages in the spleen. Heme oxygenase then degrades heme groups and

[a] *Department of Biochemistry and Biophysics, Texas A&M University, College Station, TX 77843, USA*
[b] *Department of Veterinary Surgery, Veterinary Medicine and Biosciences, College Station, TX 77843-4475, USA*
[c] *Department of Chemistry, Texas A&M University, College Station, TX 77843-3255, USA. E-mail: Lindahl@chem.tamu.edu; Fax: +1-979-845-4719; Tel: +1-979-845-0956*

† Electronic supplementary information (ESI) available: Appendix S1, additional surgical details; Fig. S1, expanded view of P1 HMM chromatographic traces in the 700 Da region; Fig. S2, LMM traces showing the effect of passing blood through the liver of iron-deficient pigs; Fig. S3, HMM traces of select isotopes of PV and CAV/CRV plasma; Fig. S4, LMM traces of select isotopes of PV *vs.* CAV/CRV plasma FLS. See DOI: 10.1039/c9mt00152b

releases iron into the blood where it migrates to the bone marrow for erythropoiesis.

Nutrient-derived Fe^{II} ions are imported into the blood through ferroportin (FPN), a membrane-bound protein on the basolateral surface of enterocytes that line the intestinal duodenum.[1–3] Also on that surface is hephaestin (HPN), a membrane-bound multicopper oxidase that catalyzes the O_2-dependent oxidation of Fe^{II} to Fe^{III}.[4] Ceruloplasmin (CPN) is a soluble multicopper oxidase in the blood that catalyzes the same reaction. The resulting nutrient-derived Fe^{III} species are released into the PV and ultimately bind apo-transferrin (apo-TFN), an 80 kDa glycoprotein in blood that serves as an iron buffer. The chemical nature of the iron species that are exported into the blood prior to coordination by apo-TFN is unestablished but it is presumed to be nonproteinaceous and LMM.

Nutrient iron import is regulated by hepcidin.[1–3] The binding of hepcidin to FPN promotes the degradation of FPN which prevents excessive influx of iron. Individuals with the iron-overload disorder hereditary hemochromatosis generate insufficient hepcidin such that excessive iron enters the blood. In this case, TFN approaches saturation (100% holo-TFN).[5] The spillover hypothesis maintains that once TFN is saturated, further iron enters the blood as one or more toxic complexes called nontransferrin-bound-iron or NTBI.[5–8] Fe^{III} citrate leads the list of NTBI candidates as the concentration of citrate in blood is high and Fe^{III} citrate is stable.[9–11] NTBI is often defined operationally as the labile iron pool in blood plasma that is chelated by a particular chelator under specified conditions. This is not ideal because different assays afford different estimates of NTBI.[12] Moreover, such assays preclude the possibility of speciating NTBI or identifying its ligands since labile iron complexes are destroyed during their detection.

Blood contains numerous iron-bound proteins besides TFN, none of which is NTBI. Haptoglobin and hemopexin bind free hemoglobin and heme in the blood, respectively.[13,14] The resulting complexes are internalized by macrophages and catabolized by the liver.[15,16] Albumin is the most abundant blood-plasma protein.[17] It reversibly binds iron but not tightly.[18–20] Serum ferritin is produced and secreted by spleen and liver macrophages, and perhaps by kidney proximal tubule cells.[21–23] Unlike intracellular ferritin, serum ferritin is not heavily loaded with Fe^{III} oxyhydroxide aggregates in its central core.[23,24] Some cells have receptors for serum ferritin, which may be involved in inflammation.[25,26]

NTBI analogs are rapidly and quantitatively absorbed by *Zip14* receptors on the plasma membrane of hepatocytes in the liver.[27–29] This organ also releases iron as needed and serves as an iron buffer. Livers of untreated hemochromatosis patients accumulate massive amounts of iron. Once the liver is iron-loaded, NTBI is absorbed by the heart and other organs, which is damaging.[30,31]

NTBI actually develops more gradually than the spillover hypothesis implies. High concentrations of NTBI have been reported in plasma in which TFN was $<45\%$ saturated.[8,32] HFE(−/−) mice, which suffer from hemochromatosis, accumulate hepatic iron even when circulating TFN is partially saturated.[4,33] TFN in 4 week old HFE(−/−) mice was only 68% saturated but the Fe concentration in their livers was 3-times normal.[34] These results imply that NTBI levels increase gradually when TFN exceeds $\sim$40% saturation. The concentration of NTBI in healthy plasma is low – only *ca.* 100 nM.[35,36] NTBI concentrations in the plasma of WT and HFE(−/−) mice were 1.5 and 3.7 μM, respectively.[6] In iron-overload diseases, the concentration of NTBI in plasma is 5–10 μM.[19,30,37]

We recently detected a half-dozen low-intensity iron-associated peaks in chromatograms of flow-through solutions (FTSs) of plasma from pigs, horses, mice, and humans with and without hemochromatosis. The masses of these species ranged from 400–2500 Da.[38] We initially assumed that they were NTBI, but their chromatography properties differed from that of Fe^{III} citrate. Also, there were no significant differences between the plasma of healthy individuals and those with hemochromatosis. Plasma iron concentrations were $\sim$1 μM, with each iron-containing species representing a few hundred nM. As a result of that study, we hypothesized that the concentrations of the LMM iron-containing species would have been higher, or additional peaks would have been observed, if the animals from which blood was drawn had eaten an iron-rich meal just prior to blood sampling AND if blood had been sampled from the PV rather than from the general circulation. We considered that the liver may have absorbed most NTBI generated after a meal and so we may not have detected this species in general circulation blood.

We designed an experiment to test these hypotheses in which catheters were surgically implanted into the PV, caudal vena cava (CAV), and/or cranial vena cava (CRV) of healthy iron-deficient pigs. Blood from these catheters were removed at various times after ^{57}Fe, a stable isotope that constitutes just 2% of natural-abundance iron, was injected into the stomach. Isotope tracing with ^{57}Fe allowed us to identify peaks associated directly with nutrient ^{57}Fe absorption. Blood containing nutrient iron from the intestines and removed from the PV did not pass through the liver. According to our hypothesis, such blood should contain high levels of ^{57}Fe-labeled NTBI. Our objective was to detect NTBI directly using liquid chromatography, and ultimately determine its chemical composition. Although this objective was not met, our results afford new insights into the iron composition of blood.

Experimental procedures

Pig acquisition and maintenance

All experiments involving pigs were approved by Texas A&M University (IACUC 2015-0034 and 2018-0204). Four female Yorkshire pigs (*Sus scrofa domesticus*) weighing *ca.* 18–23 kg were purchased locally, one at a time. Upon arrival at TAMU, pigs 1, 2, 3 and 4 (named P1, P2, P3, and P4) were placed on an iron-deficient swine diet (Envigo Inc. Rx 2096077; TD.150728) and quarantined 3 week in a relatively iron-deficient pen with a cement floor and aluminum bars. P2 arrived with a minor abscess on its right rear leg which was treated with topical

ointment and allowed to heal completely, as determined by veterinary staff at TAMU, prior to use in this study. P2 was fed the iron deficient diet for 3 weeks, identical to the other animals. P1, P2, and P3 were conditioned to be comfortable with humans through daily interactions. P4 was additionally trained to be suspended in a custom-built neoprene-coated nylon (McMaster-Carr) sling for extended periods.

Surgery and recovery procedures

Pigs were placed under general anaesthesia, and a feeding tube was installed into the stomach, a polyethylene catheter was installed into the PV, and an identical catheter was installed into either the CAV (P2 and P3) or the CRV (P1), using a procedure similar to that described.[39,59,60] For P4, a venous-access port (VAP, ClearPort Max, Access Technologies, Skokie, IL) was installed in the PV and CAV.

The PV catheter was placed caudal to the bifurcation of the two branches leading into the liver.[61] The distal end of the catheter exited the abdomen and was secured to the neck of the animal for sampling. The CAV catheter was inserted in the femoral vein and advanced into the caudal vena cava.[39] The distal end of the catheter was secured to the animal's back for sampling. Additional surgical details are given in ESI.†

The ^{57}Fe import experiment

After P1, P2, and P3 recovered for 3 days, and P4 recovered for 14 days (due to the VAPs), each pig was fasted 24 h. During the fasting day, 10 mL of an 80 mM ^{57}Fe solution (prepared by dissolving 95.5% enriched ^{57}Fe metal (Isoflex USA) in trace metal grade aqua-regia) was mixed in an anaerobic glove box (Mbraun Labmaster 120) with 10 mL of 800 mM sodium ascorbate, generating a 40 mM ^{57}Fe and 400 mM ascorbate stock solution that was stored in the glove box overnight. The iron in other samples prepared in the same way was in the ferrous state as demonstrated by Mössbauer spectroscopy. The difference in recovery times was due to use of either a catheter or a VAP.

On the morning after the fast, P1, P2, and P3 were immobilized in an aluminum restraint cage and P4 was placed in the sling. Blood samples were removed from each catheter using either 6 or 10 mL plastic disposable syringes. Samples were transferred to 1–2 lithium-heparinized 6 mL vacutainer tubes (BD Vacutainer, #36788) and placed on ice. These "pre-injection" samples were centrifuged at 2000 × *g* for 12 min immediately after blood was collected. Plasma was collected using a plastic Pasteur pipette, transferred to labeled Eppendorf tubes, and frozen immediately in liquid N_2.

At the beginning of the iron-import kinetic experiment (t = 0), 20 mL of the stock ^{57}Fe solution was injected into the stomach *via* the feeding tube. Aliquots of blood were removed from each catheter at t = 2, 5, 10, 15, 25, 60, and 100 min post-injection, transferred to vacutainer tubes, and placed on ice. At the end of the experiment, pigs were exsanguinated using Ringer's buffer to remove residual blood.

Individual animals were treated slightly differently. P1 was given the anaesthetic Telazol shortly after injection of ^{57}Fe to calm it enough for reliable sample collection. Also during surgery, the caudal vein was inaccessible in that animal so the cranial vein was used instead. P3 was given anaesthetic early in the experiment to allow the surgical repair of the PV catheter which had unintentionally kinked. For P4, VAPs were used instead of catheters to minimize the kinking problem. However, prior to injection of ^{57}Fe into the stomach the PV VAP unintentionally clogged. P4 was sedated for installation of an ear catheter which was used to infuse 125 mg of ferric gluconate (Santofi-Aventis, Ferrlecit) in 50 mL of saline. This was done intentionally in an effort to saturate transferrin and generate higher levels of NTBI after ^{57}Fe injection. The solution flowed into P4 at a rate of 0.52 mg Fe per min using a syringe infusion pump (B. Braun). The infusion began 2 h prior to injecting ^{57}Fe and ended *ca.* 40 min thereafter. P4 was lightly sedated during the infusion and subsequent experiment. The animal was suspended in the sling for infusion and sample collection.

Plasma processing

The blood samples that had been placed on ice during the experiment were centrifuged as above as soon as possible. The plasma layer was removed, transferred to a 2 mL Eppendorf tube, and frozen immediately in liquid N_2. At different times after the experiment, individual plasma samples were thawed and brought into a chilled anaerobic glove box (MBraun Labmaster 120, 1–10 ppm O_2, 4–8 °C). Measured volumes of plasma (1–2 mL) were concentrated using a stirred-cell (Amicon Model 8003) with a regenerated cellulose 10 kDa cut-off membrane (Millipore Sigma, PLGC02510). Approximately 3/4ths of the initial volume was collected as flow-through solution (FTS) which was immediately injected onto a chromatography column. Low-molecular mass analysis was performed on two Superdex Peptide 10/300 GL (GE Healthcare, 17517601) columns connected in series. For high-molecular mass analysis, frozen plasma samples were treated identically except that they were filtered outside of the glovebox using either a 0.2 μm cellulose acetate membrane or a 0.45 μm PES membrane (VWR). The filtrate was returned to the glovebox and immediately injected onto a single Superdex 200 10/300 GL column (GE Healthcare, 17517501). The mobile phase for both columns was 20 mM ammonium bicarbonate (Fisher Scientific) pH 8.5 that had been degassed using a Schlenk line prior to import into the box. Flow through the column was driven by a Bioinert LC (Agilent 1260 Bio-Inert Quaternary pump with diode array, fraction collector, and manual injection valve) located inside the glove box. Eluate flowed to an ICP-MS (Agilent 7700x) outside of the box and detected for ^{56}Fe, ^{57}Fe, and other metals as described.[62] Superdex peptide size exclusion columns were calibrated as described.[62] The Superdex 200 size exclusion column was calibrated by running bovine thyroglobulin (660 kDa, Sigma-Aldrich), equine splenic apo-ferritin (470 kDa), soybean beta-amylase (200 kDa, TCI America), recombinant-equine alcohol dehydrogenase (150 kDa, Sigma-Aldrich), human transferrin (80 kDa, Athens Research and Technology), carbonic anhydrase (29 kDa, Sigma), and cyanocobalamin (1.3 kDa, Fisher BioReagents). These standards were brought up in 20 mM Tris-base (Fisher) and 10 mM NaCl (EMD) and were filtered with either a 0.2 or

0.45 μm syringe filter (VWR) prior to injection. The Superdex 200 column had a void-volume V_0 of 8.1 mL. The column was calibrated by plotting the logarithm of the standard molecular weight *vs.* elution volume V_e/V_0. The best-fit linear-regression line was log(mol. wt) = $-1.7612(V_e/V_0) + 7.7225$ with an R^2 of 0.992. All columns were cleaned at the end of the day as described.[62]

Quantitative elemental analysis

Frozen plasma was thawed and 3 aliquots of 50–100 μL each were placed in new 15 mL plastic screw-top Falcon tubes. Concentrated trace-metal-grade nitric acid (120 μL) was added to each tube. The tubes were capped and sealed using electrical tape. Samples were placed in an oven at 70–80 °C for 12–14 h. After digestion, samples were cooled for >1 h, diluted with high-purity water to 6.00 mL, and then analyzed by ICP-MS.

Transferrin saturation assay

The total iron binding capacity (TIBC) assay was performed by Texas Veterinary Diagnostic Laboratory using a Beckman Coulter AU analyzer. The TIBC assay used both the total iron concentration assay and the unsaturated iron binding capacity assay.

Iron binding proteins

Standard buffer consisted of 25 mM sodium bicarbonate (Fisher), 20 mM Tris-base (Fisher), and 10 mM NaCl (EMD), prepared in high purity water and adjusted to pH 7.4 using trace-metal grade HCl (Fisher). Stock solutions of transferrin (Athens Research and Technology) (76 μM) and bovine serum albumin (Sigma) (1.2 mM) were prepared in the standard buffer with or without ferric citrate (70 μM). A 40 mM stock solution of Fe^{III} citrate was prepared by mixing ferrous ammonium sulfate (Fisher) and three molar equivalents of sodium citrate (Fisher) in deionized water. The resulting pH was adjusted to 5 using citric acid (Acros Organics); final concentrations were obtained using deionized water. Transferrin and iron were mixed at a molar ratio of 1 : 1, and albumin and iron were mixed at a molar ratio of 1 : 0.058. Resulting solutions were mixed, incubated for 1 h, then passed through a 0.2 μm filter (VWR). Solutions of transferrin, with or without iron added, were mixed 1 : 1 (volume ratio) with solutions of albumin with or without iron added. Control solutions were mixed 1 : 1 with buffer. A solution of alcohol dehydrogenase (Sigma) was prepared (10 mg mL^{-1}) in standard buffer, and mixed in a 1 : 1 : 1 volume ratio with stock solutions of Fe^{III} transferrin (prepared using Fe^{III} citrate) and albumin. Ferritin (Sigma; 2 mg mL^{-1}) was prepared in standard buffer except lacking bicarbonate. These solutions were then passed though the Superdex 200 GL column as described above.

Results

Metal content of plasma *vs.* FTSs

Metal concentrations in filtered plasma from the PV and from the CAV/CRV were similar (Table 1); ^{56}Fe + ^{57}Fe concentrations ranged from 10–30 μM. FTSs from plasma contain ≤1 μM iron,[38] indicating that only 3–10% of the iron species in the filtered plasma of iron-deficient pigs have masses <10 kDa. The $^{57}Fe/^{56}Fe$ ratio in filtered PV plasma from P1, P2, and P3 (and in the CAV plasma of P4) increased significantly over the 100 min experiment (Fig. 1, top). The P1 $^{57}Fe/^{56}Fe$ concentration ratio increased immediately after injection whereas the P2–P4 ratios increased after a 5–15 min lag. Enrichment was observed for all animals, but the enrichment in P1 was highest. The ^{56}Fe concentration in P1 plasma increased slightly after ^{57}Fe injection, perhaps as a secondary response to injection. The ^{57}Fe enrichment of P4 plasma may have been low due to the $^{56}Fe^{III}$ gluconate infusion prior to the ^{57}Fe injection. This infusion may have elicited a secondary response that attenuated ^{57}Fe intestinal absorption.

Kinetics of iron import

We quantified the kinetics of iron import from the stomach, through the intestines, and into the blood, assuming the sequential reactions $^{57}Fe_{stomach} \xrightarrow{k_1} {}^{57}Fe_{emterocytes} \xrightarrow{k_2} {}^{57}Fe_{plasma}$. k_1 and k_2 are apparent first-order rate-constants for the transfer of iron from the stomach to the intestines, and from the intestines to the blood, respectively. Simulations were generated (in IgorPro) using eqn (1)

$$\left[{}^{57}\mathrm{Fe}\right]_{\mathrm{plasma}} = a\left(1 + \frac{k_1 e^{-k_2 t} - k_2 e^{-k_1 t}}{k_2 - k_1}\right) + c \qquad (1)$$

where a is an empirical fitting parameter that scales the time-dependent response and c is an empirical off-set parameter that

Table 1 Average metal and phosphorus concentrations in blood plasma from the portal vein and either the caudal or cranial vein. Values reported for each pig are the average of time points before and after ^{57}Fe injection. Values are the average of n = 4–10 independent samples collected at different times during the experiment. Concentrations of Mn and Co were below detection. Corresponding ^{57}Fe values are in Fig. 2

	Portal vein			Caudal (CAV) or cranial (CRV) vein			
Element	P1	P2	P3	P1	P2	P3	P4 (CR)
Replicates	9	9	9	9	4	9	9
^{56}Fe (μM)	8 ± 3	8 ± 4	7 ± 1	8 ± 5	11 ± 7	9 ± 2	160 ± 40[a]
Cu (μM)	32 ± 4	26 ± 2	19 ± 2	32 ± 2	21 ± 1	18 ± 1	32 ± 2
Zn (μM)	5 ± 2	13 ± 1	11 ± 2	7 ± 7	12 ± 1	11 ± 1	14 ± 1
Mo (nM)	30 ± 30	20 ± 10	40 ± 5	10 ± 10	10 ± 4	40 ± 7	20 ± 2
P (mM)	6 ± 1	4 ± 0.1	4 ± 0.3	6 ± 1	3 ± 0.1	4 ± 0.3	5 ± 0.2

[a] In P4, the high concentration of ^{56}Fe is due to ferric gluconate infusion. The significant uncertainty in iron concentrations may be due to variable levels of hemolysis.

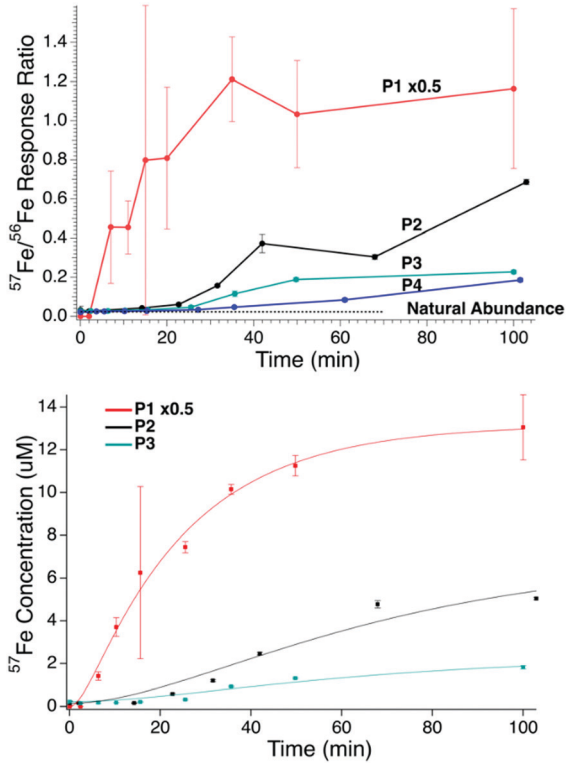

Fig. 1 Top panel: Ratio of ^{57}Fe/^{56}Fe concentrations in plasma samples obtained from the PV of P1, P2, and P3, and the CAV of P4 at different times after ^{57}Fe injection into the stomach. Traces: red, P1; purple, P2; green P3; blue P4. Dashed black line is the ratio of natural abundance of ^{57}Fe/^{56}Fe. Error bars are standard deviations. Bottom panel: Plot of ^{57}Fe concentration of PV plasma *vs.* time after injecting ^{57}Fe^{II} into the stomachs of P1 (red), P2 (black), and P3 (green). Solid lines are simulations obtained using eqn (1) and the parameters in Table 2. The intensity of the P1 plot was reduced 2-fold (×0.5).

Table 2 Best-fit parameters used to fit eqn (1) to plots of ^{57}Fe in plasma *vs.* time after injecting ^{57}Fe^{II} ascorbate into the stomach of pigs P1, P2 and P3

Animal	k_1 (min^{-1})	k_2 (min^{-1})	a (μM)	c (μM)
P1	0.043	0.340	26	0
P2	0.029	0.027	6.7	0.15
P3	0.027	0.034	2.1	0.22

shifts simulations vertically. Simulations were fitted to plots of [^{57}Fe] in the PV plasma *vs.* time after injecting ^{57}Fe into the stomachs of P1, P2 and P3 (Fig. 1, bottom solid lines). Optimal k_1 values (Table 2) were similar for all datasets whereas k_2 values were more variable. This implies that the rate of iron absorption from the stomach to the intestines is similar from one animal to the next whereas the rate of iron import from the intestines to the blood is more variable.

Chromatography of standards

Before investigating the ^{57}Fe-containing species in the plasma, we passed authentic candidate proteins down the same columns and used the same chromatography conditions. Horse spleen ferritin (470 kDa) migrated as two peaks (Fig. 2A). The first peak

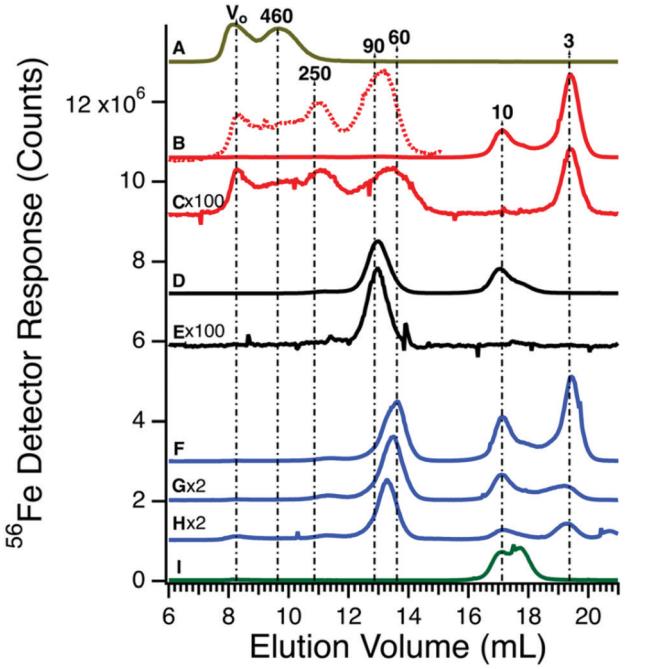

Fig. 2 Iron-detected chromatograms of high-molecular mass protein standards. (A) Ferritin (4.4 μM, 450 kDa); (B) albumin (600 μM, 60 kDa) plus 0.06 molar equivalents of Fe^{III} citrate. The dotted line is a 100-fold expanded view; (C) albumin (600 μM); (D) transferrin (36 μM, 80 kDa) after incubating with Fe^{III} citrate (36 μM); (E) transferrin (36 μM); (F) transferrin (36 μM), albumin (600 μM), and Fe^{III} citrate (72 μM); (G) same as F except 36 μM Fe^{III} citrate; (H) transferrin (25 μM), albumin (400 μM), alcohol dehydrogenase (22 μM), and Fe^{III} citrate (25 μM); (I) Fe^{III} citrate (72 μM). All concentrations listed are final. The intensity of the indicated traces were multiplied by 100 and 2 (×100 and ×2), respectively.

corresponded to the void volume (V_0) while the second peak corresponded to a mass of 460 kDa. The V_0 peak may reflect aggregated ferritin species. Bovine serum albumin (66.5 kDa) binds iron weakly, but its concentration in blood is high (*ca.* 700 μM) such that it might be a significant iron-binding protein.[39] Albumin incubated with *ca.* 0.06 molar equivalents of Fe^{III} citrate exhibited low-intensity iron-detected peaks at V_0, 250, 90, 10, and 3 kDa (Fig. 2B and Fig. S2, ESI†). Peaks at 10 and 3 kDa reflect excess iron not bound to albumin; the 10 kDa peak was also observed when Fe^{III} citrate was run alone (Fig. 2I). Peaks at V_0 and 250 kDa may reflect albumin aggregates. An albumin sample that was not incubated with iron exhibited iron-detected peaks at V_0, 250, 90, and 3 kDa (the 10 kDa peak due to Fe^{III} citrate was absent) (Fig. 2C). However, intensities were diminished relative to those incubated with iron. Human TFN (80 kDa) incubated for 1 h with 1 molar equivalent of Fe^{III} citrate migrated according to a mass of 90 kDa (Fig. 2D); the peak at 10 kDa was likely due to excess Fe^{III} citrate. TFN without added iron exhibited the 90 kDa peak (Fig. 2E) at lower intensity.

We were concerned that the similar migration rates of iron-bound albumin and TFN would complicate our analysis. However, the intensity of the albumin peak was much less than that of TFN (even at the 700 : 1 albumin : TFN molar protein concentration ratio), indicating that any plasma peaks in this

mass region are essentially due to TFN. To examine whether the two proteins could be distinguished chromatographically, TFN and albumin were mixed (with added Fe^{III} citrate) to a final concentration similar to those of the individual standards in Fig. 2B and D. Interestingly, the TFN peak shifted to an apparent mass of *ca.* 60 kDa (Fig. 2F). Repeating the experiment with iron added only to the TFN (half as much iron, overall) yielded similar results (Fig. 2G). The shift may be due to secondary interactions of albumin acting at high concentrations as a pseudo-salt. The mobile phase contained minimal salt and so an albumin-dependent salting-effect may have caused a significant perturbation. We examined the effect of albumin on the elution of TFN by reducing the final concentration of albumin in trace H of Fig. 2. This shifted the elution volume of TFN towards that in the absence of albumin, supporting our explanation.

Chromatograms of high-molecular mass (HMM) plasma

HMM traces of filtered plasma from P1 and P2 are shown in Fig. 3 (A → F for P1 and G → I for P2). In both experiments, 2–4 dominant ^{56}Fe peaks (red lines) were observed before (A and G) and after (B–F and H) injecting $^{57}Fe^{II}$. For the P1 experiment, dominating peaks corresponded to masses of 200 kDa and 50–20 kDa. A low-intensity peak in the 700 kDa region was also present (Fig. S1, ESI†). The 50–20 kDa region consisted of three partially resolved peaks. This was likely due to different forms of TFN. Apparent masses are lower than in traces of purified TFN (85 kDa) and in traces of TFN mixed with albumin (60 kDa). Albumin and other proteins and salts in filtered plasma probably shifted the TFN peaks.

P2 traces exhibited similar peaks except that the 700 kDa peak was more intense. The 50–20 kDa region was similarly composed of three unresolved peaks. The 700 kDa peak was probably due to serum ferritin as we are unaware of other iron-containing proteins in the plasma with such a high mass; recall that authentic ferritin exhibited a peak at V_0. The peak at 200 kDa is probably due to haptoglobin since we previously determined that authentic haptoglobin migrated in accordance with this mass.[38] The variable intensity of this peak probably reflects a variable extent of hemolysis during sample collection.

Ideally, the ^{56}Fe traces associated with P1 and P2 (Fig. 4, red lines) would have been invariant in terms of species and intensities, since we did not inject ^{56}Fe into the animals. That expectation was generally realized, but not entirely so. The first four LMM ^{56}Fe traces of the P1 FTS (Fig. 3A–D) were essentially invariant but at longer times, the ^{56}Fe peak intensities increased (data not shown). A similar phenomenon was observed for P2 (compare Fig. 3, G *vs.* H). Perhaps ^{56}Fe was released (after ~30 min delay) from internal bodily stores (*e.g.*, macrophages in the liver and spleen) in response to injecting ^{57}Fe into the stomach.

Prior to injecting ^{57}Fe into P1 and P2, the $^{57}Fe/^{56}Fe$ concentration ratio associated with each of the 2–3 major LC peaks was defined to be natural abundance (2%/94%). For the same peaks obtained from a sample collected 35 min after injecting ^{57}Fe into P1's stomach, the ratio associated with the TFN peaks in the 50 kDa region was significantly higher than natural abundance (Fig. 3E). The same was observed in filtered plasma

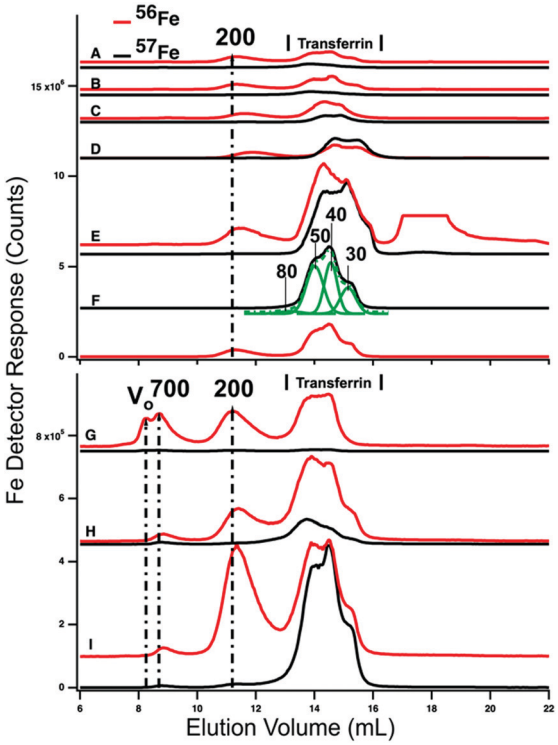

Fig. 3 High-molecular mass LC-ICP-MS chromatograms of PV plasma. Plasma from P1 and P2 were passed through a 0.2 μm filter and then chromatographed. Top panel, P1: (A) pre-injection; (following times all post-injection) (B) 2 min; (C) 10 min; (D) 16 min; (E) 36 min; and (F) 100 min. Bottom panel, P2: (G) pre-injection; (H) 14 min; (I) 100 min post-injection. Red and black lines are ^{56}Fe and ^{57}Fe, respectively. In the red trace E, an unidentified peak at *ca.* 18 mL was truncated. The ^{57}Fe trace F was fitted for four Gaussian (solid green) peaks which produced a resultant green-dashed trace. FitYK was used in fitting.[63] Assigned peaks are in kDa.

collected 100 min after ^{57}Fe injection into P2 (Fig. 3I). Neither the putative ferritin nor haptoglobin peaks had elevated $^{57}Fe/^{56}Fe$ ratios. This demonstrates that the ^{57}Fe injected into the stomach bound apo-TFN as it entered the PV, but did not bind other iron-containing proteins. The iron bound to these other iron-containing proteins obviously originated from nutrient iron, but the import and binding must have occurred well before the current experiment. The ability of apo-TFN to bind nutrient-derived ^{57}Fe also indicates that the TFN buffer system was not saturating in P1–P4 experiments. P4 had the lowest extent of ^{57}Fe enrichment probably because the $^{56}Fe^{III}$ gluconate infusion increased TFN saturation to 60%.

The serum ferritin peaks in Fig. 3G represented ~30% of the iron in the sample (ignoring the 200 kDa peak) whereas the same peak in Fig. 3H (sampled from the same catheter ~14 min later) was half as intense. The trace of Fig. 3G matches Fig. 5D except that blood was removed from the PV rather than CAV. The serum ferritin peak in Fig. 3G is significantly stronger, implying that the liver absorbed some serum ferritin iron.

Chromatograms of FTSs

We also examined FTSs from the same plasma samples using an LC column that resolved LMM species. For P1, chromatograms

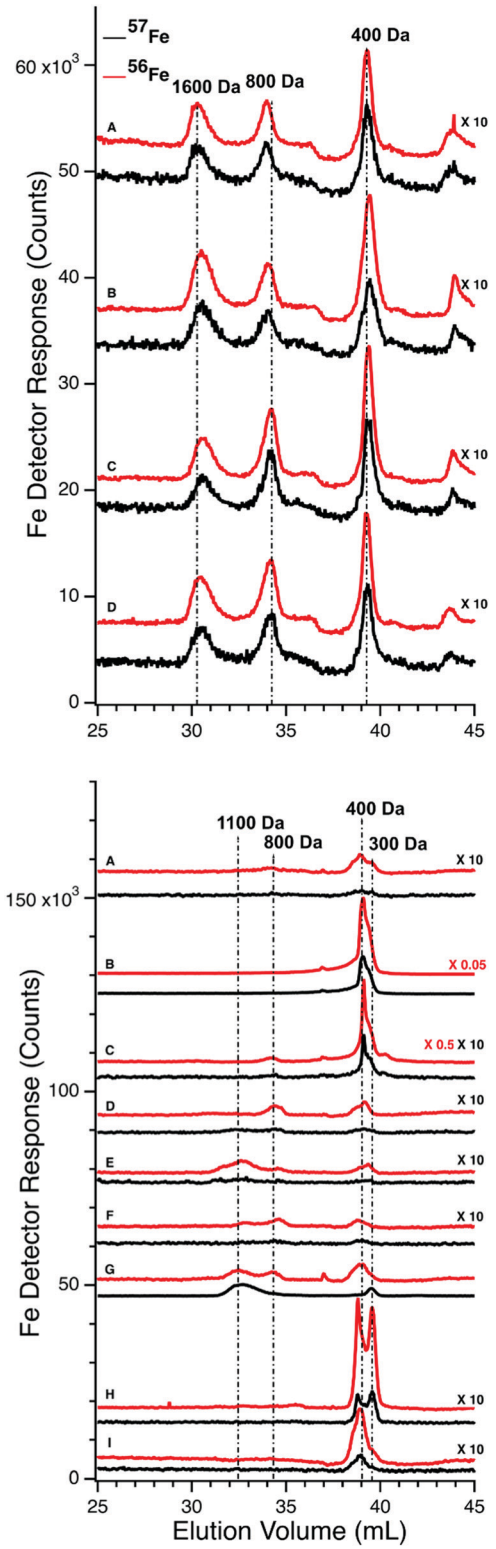

Fig. 4 Low-molecular mass LC-ICP-MS chromatograms of FTS of PV (upper panel) and CRV (lower panel) plasma from experiment P1. Upper panel: (A) prior to injection of ^{57}Fe into the stomach; (following times all post-injection) (B) 6 min; (C) 10 min; (D) 26 min. Red and black traces indicate ^{56}Fe and ^{57}Fe, respectively. ^{57}Fe traces were magnified 10-fold. Lower panel: (A) prior to injecting ^{57}Fe into the stomach; (following times all post-injection) (B) 2 min; (C) 6 min; (D) 10 min; (E) 15 min; (F) 26 min; (G) 36 min; (H) 50 min; and (I) 100 min. Red and black traces indicate ^{56}Fe and ^{57}Fe, respectively. Indicated traces were magnified by factors of 10, 0.5, or 0.05.

of the FTSs from the PV and the CRV were obtained (Fig. 4, top and bottom panels, respectively). The collective intensity of the observed iron-associated peaks was far less than for the HMM iron species in filtered plasma, reflecting the lower concentration of LMM iron in plasma. In the PV FTS, major iron-associated peaks were present at masses 1600, 800, and 400 Da (Fig. 4). Their intensities were invariant between the time at which the control PV FTS sample was collected and at 35 min post-injection. At later times, the higher-mass LMM species were not always present whereas the 400 Da peaks were routinely present. Similar results were obtained for PV FTSs in the P2 and P3 experiments, where the predominate species observed was at 400 Da (Fig. S2, ESI†). For P2 and P3, peaks in the 400 Da region dominated, followed by peaks at 1500 and 1200 Da (Fig. S2, ESI†). The same species were present before and after ^{57}Fe injection. The intensities of the P2 peaks were more scattered than those for P1, and no time-dependent trends were evident. For P3, the major peak was also in the 400 Da region but it was broadened and less resolved. A minor-intensity peak in the 1700–1500 Da region was evident in the pre-injection trace, but not in subsequent traces. The peak intensity in the 400 Da region was variable but with no obvious time-dependence. We also monitored other metals in our plasma samples and observed reproducible peaks for P, S, Mn, Co, Cu, and Zn (Fig. S3 and S4, ESI†).

Effect of liver

We expected that the liver would absorb one or more of the detected LMM iron species as blood from the PV passed through it. That expectation was not fully realized. ^{56}Fe traces of FTS from the PV and CRV of P1 are shown in Fig. 4, upper and lower panels, respectively. Similar results were observed for the CAV for P2 and P3. For the pre-injection trace of CRV plasma, the 400 Da region was significantly more intense than in the PV trace, but it lacked the 1600 Da species. The 800 Da species in the PV was present in some CRV traces (Fig. 4, lower panel, traces C, D, and F) but not in others (trace A). Peaks were reproducibly present in the 400 Da region, similar to in our previous study in which we referred to this region as the "anchor".[38] Differences for the P2 and P3 experiments were also variable (Fig. S2, ESI†) in that the intensities of the 400 Da peaks in some samples were greater in the CAV trace than in the corresponding PV trace, whereas in other samples the opposite was observed.

The liver had a stronger effect on TFN. Using the HMM column, chromatograms of filtered plasma from the PV and CAV/CRV differed in the shape of the TFN peaks (Fig. 3 *vs.* Fig. 5). For PV traces, the TFN region exhibited three semi-resolved peaks (Fig. 3), with apparent masses between 50–30 kDa. Simulations indicate a 3 : 2 : 1 ratio (in terms of iron detection). TFN has different glycosylated isoforms which are altered by the liver.[40–44] We suggest that the different peaks reflect different levels of glycosylation; this caused distinct elution profiles in other chromatography studies.[45,46] The TFN peaks in P1, P2, and P3 CAV/CRV plasma samples were more homogeneous (Fig. 5), with the 50 kDa species dominating. The extent of ^{57}Fe enrichment

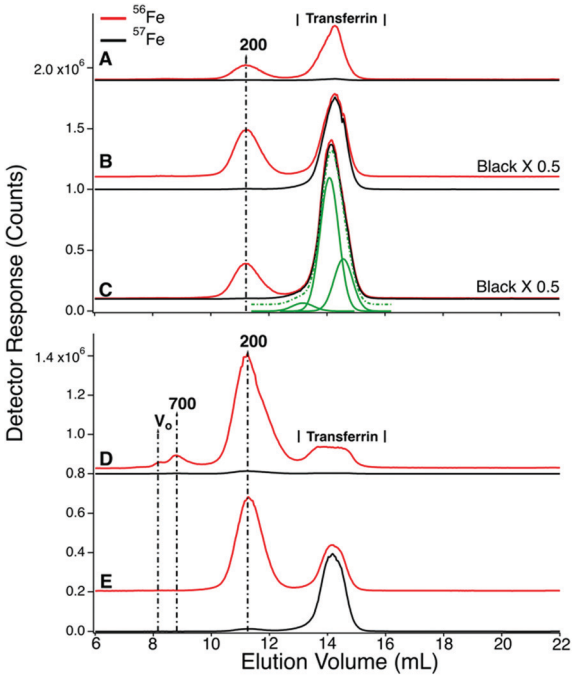

Fig. 5 High-molecular mass chromatography traces of filtered plasma from the CAV and CRV. Traces A–C are from P1. (A) Pre-injection (before injecting ^{57}Fe into the stomach); (B) 28 min post-injection; (C) 101 min post-injection. Traces D and E are from P2; (D) pre-injection, (E) 63 min post-injection. Assigned peak masses are in kDa. A detector switch artifact was removed electronically from the 200 kDa peak in trace D. Trace C was fitted with three (solid green) Gaussian lines which summed to give the dashed line. Simulations used FitYK software.

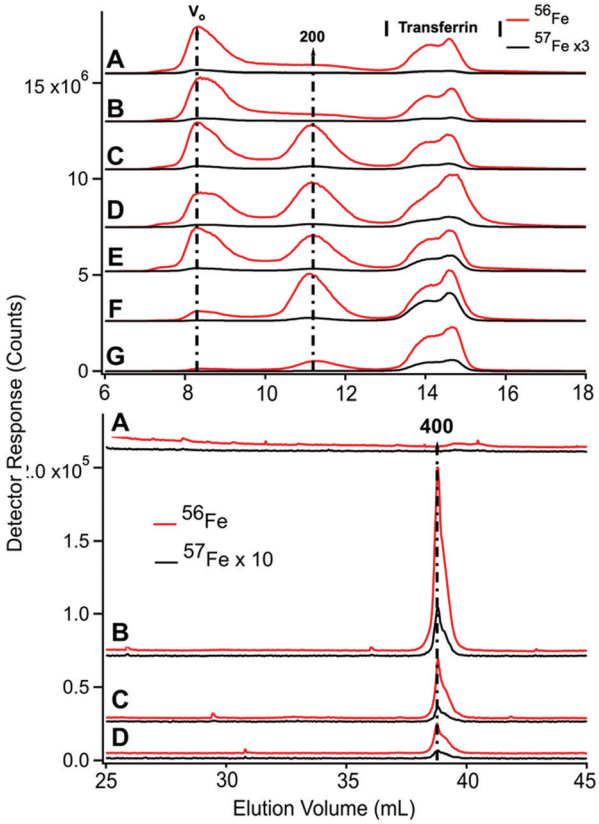

Fig. 6 Low-molecular mass (upper) and high-molecular mass (lower) of LC-ICP-MS chromatograms of filtered CAV plasma from P4. Upper panel; analysis of filtered plasma. (A) Prior to injection of ^{57}Fe into the stomach; (B) 4 min; (C) 15 min; (D) 25 min; (E) 35 min; (F) 60 min; (G) 100 min post-injection. Red and black lines are ^{56}Fe and ^{57}Fe, respectively. Lower panel; analysis of FTS. (A) prior to injection of ^{57}Fe into the stomach; (B) 10 min; (C) 36 min; (D) 102 min post-injection. The intensities of indicated traces were reduced two-fold (×0.5).

and the overall concentration of ^{57}Fe in the CAV/CRV were not significantly different relative to the PV. Thus, it appears that the liver processes different forms of TFN in a manner that renders them more homogeneous. The results of the P4 experiment were more difficult to assess because PV blood was not obtained. Here, the TFN peaks in traces of CAV filtered plasma (Fig. 6, top panel) exhibited two isoforms. However, P4 was infused with ferric gluconate, and the effect of the liver might have changed.

Partial saturation of transferrin did not generate new nutrient-derived LMM Fe species

We attempted to saturate TFN in P4 blood by infusing the animal with $^{56}Fe^{III}$ gluconate for 2 h prior to injecting $^{57}Fe^{II}$ into its stomach. The infusion continued for 40 min after injection. Excess ferric gluconate nanoparticles (250–440 kDa) were observed at V_0 in traces of filtered P4 plasma from the CAV (Fig. 6, upper panel, 8.2 mL). The peak was observed before (trace A) and after (traces B–E) injection. Soon after the infusion ceased, the intensity of that peak declined sharply (traces F and G) indicating rapid absorption by the body – probably by the liver. We estimate $t_{1/2}$ to be ~30 min for this process.

In the same ^{56}Fe traces of Fig. 6, the intensities and shapes of the TFN region at 50 kDa were largely invariant. The intensity of the same peaks in the ^{57}Fe traces increased as expected at increasing times after injecting ^{57}Fe into the stomach. Similar to that observed in P1 and P2 experiments, the other peaks in the chromatograms did not become enriched in ^{57}Fe.

Due to the effects of ferric gluconate, TFN saturation levels were higher than normal; saturation levels were 50%, 71%, 80% and 59% at 0, 25, 60, and 100 min. The 25 and 60 min samples exhibited hemolysis which might have artificially increased saturation measurements. More accurate values are probably 50–60%, similar to the other time-points in the series.

LMM analysis of these samples showed no ^{57}Fe enrichment beyond natural abundance (Fig. 6, bottom graph, A–D). However, PV samples could not be collected for the P4 animal and enriched species could have been generated in the PV but quantitatively absorbed by the liver so as to be absent in the CAV. We consider this unlikely because the LMM species in the FTS of PV plasma from P1 (which showed the highest ^{57}Fe enrichment after injection) were not enriched, even though saturation levels were reasonably high. Saturation levels were 8% at pre-injection, 34% at 25 min post-injection, and 64% at 100 min post-injection (all in the CAV). Although these levels were quite high towards the end of the experiment, the LMM iron-detected peaks in corresponding samples were not ^{57}Fe-enriched nor were they more intense

than in samples from earlier timepoints. Since the liver absorbs TFN, saturation levels could have been even higher in the PV of P1 after injection (and still there was no enrichment of LMM iron species in the PV).

Discussion

Our objective was to detect NTBI in blood plasma using liquid chromatography rather than the more common method of chelator binding and iron-sensitive colorimetric assays. We expected that NTBI would consist of one or more LMM iron complexes derived from nutrient iron and that these complexes would enter the blood prior to binding apo-TFN. We expected that the concentration of NTBI would vary with the saturation of TFN, and that NTBI would be absorbed by the liver such that there would be major differences between PV and CAV/CRV plasma. We tried to increase the intensity of previously detected LMM species (and/or discover new LMM iron species that might be NTBI) by injecting ^{57}Fe into the stomachs of iron-deficient pigs and then removing blood before and after passage through the liver. Despite these efforts, none of our expectations was realized. Our conclusions are outlined in the model of Fig. 7 and in the following paragraphs (with the major conclusion highlighted).

Most iron in healthy nonhemolyzed blood plasma is bound to TFN; a variable percentage is bound to serum ferritin and a small percentage (3–10%) is present as 2–4 LMM iron species

Iron-peaks at ~200 kDa were assigned to the haptoglobin: hemoglobin complex but its intensity varied as expected if different samples experienced different levels of hemolysis. Thus, we view the 200 kDa peaks as sampling artifacts.

The only other HMM iron-containing peak in plasma (eluting at or near V_0) was assigned to iron-loaded serum ferritin monomers or aggregates. The intensity of this peak varied from 0% to 40% of plasma iron. This high level of variability was observed in the same animal, sometimes in samples obtained within *ca.* 10 min of each other. These results support a turnover rate of serum ferritin on the order of minutes as reported previously.[47,48] Our results are consistent with the use of serum ferritin as a signal involved in acute phase response.[49]

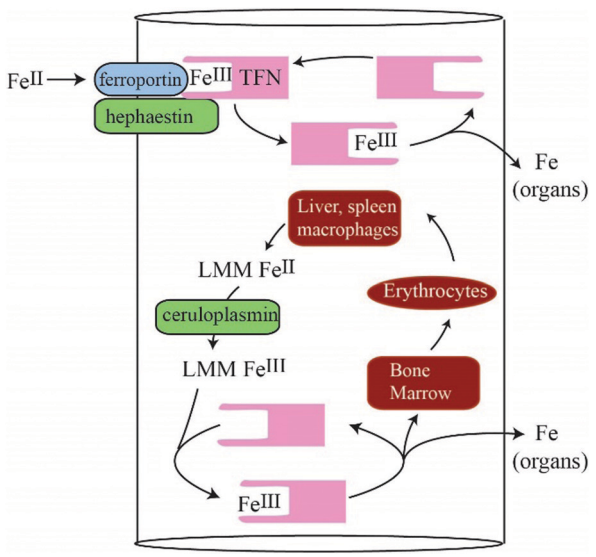

Fig. 7 Model for LMM iron trafficking in healthy blood: nutrient iron is imported through FPN, oxidized by HFN, and transferred to apo-TFN in a channelled step in which no Fe^{III} intermediate forms. During red-cell recycling, low-mass Fe^{II} species from liver and kidney macrophages are proposed to be released into the blood. They become oxidized by CPN to the Fe^{III} state, coordinated to apo-TFN, and then trafficked to the bone marrow for erythropoiesis as well as to organs as needed. The proposed LMM $Fe^{II/III}$ intermediates may be those detected in this study.

The detected LMM Fe species in plasma coexist with apo-TFN, a strong chelator of Fe^{III} ions

The iron species either do not bind apo-TFN or they bind it weakly and reversibly.[38] Assuming the simplistic reaction {Fe + apo-TFN ⇄ TFN} where [Fe] ≈ 0.2 μM and [apo-TFN]/[TFN] ≈ 0.7/0.3, suggests that K_d ≈ 0.5 μM which is not as tight as assumed for iron binding to TFN.

Nutrient-derived iron that enters the blood binds apo-TFN directly (*i.e.*, channeled from FTN to apo-TFN) without passing through a long-lived LMM Fe intermediate

Otherwise, we would have detected ^{57}Fe enriched LMM iron species in plasma (unless such species were absorbed onto the chromatography column – a possibility that we cannot rigorously exclude). There is some support in the literature for complex formation of the relevant proteins and perhaps channelling. FPN physically interacts with HPN and CPN.[51,52] FPN and HPN both migrate from the apical to basolateral surface of enterocytes. The rate of ^{55}Fe efflux from Xenopus oocytes increases in the presence of apo-TFN and CPN[53–56] consistent with an interaction with FPN. Fe^{II} binding to FPN may stimulate a conformational change that releases cytosolic Fe^{II} into the blood.[54] CPN helps remove Fe^{II} from FPN; otherwise the Fe^{II} remains on FPN.[57] FPN may act "in concert" with HFN and/or CPN to release Fe.[58] An advantage to channelling is that aqueous Fe^{II} ions would not be present in the blood of healthy individuals, preventing ROS-based reactions. Channels are probably tightly regulated. The LMM iron complexes observed here may not cause excess ROS damage because they are tightly coordinated, in the ferric state, or present at low concentrations.

The LMM Fe species detected in mammalian blood plasma are NOT derived directly from nutrient absorption but rather from internal iron stores

Such stores might include Kupffer macrophages in the liver and/or red pulp macrophages in the spleen. Both degrade red blood cells as a part of red-cell recycling, a process that involves far more iron and higher flux rates than nutrient iron import.[50] These macrophages could have released the observed LMM iron species. Another possibility is that the detected iron species were exported by FPN in erythrocytes or erythroblasts.[42]

The iron-deficient liver has a modest effect on LMM and HMM iron species; it seems to release iron species with masses in the 400 Da region and absorb iron species in the 500–1500 Da region. It also alters the observed isoforms of TFN

The liver probably rapidly removed the ferric gluconate in the blood, as was observed after infusion was halted. The liver acts as an iron buffer to store and mobilize iron as needed.[50]

The intensity of the detected LMM iron species is not correlated to the level of transferrin saturation in the range between 8% and 60%

In all cases, the intensity of the LMM species was low and uncorrelated. This surprising result is difficult to reconcile with a gradual spill-over mechanism. We cannot exclude the possibility that the intensity of these LMM plasma irons species would increase dramatically at higher saturation. More likely is that they are not directly associated with nutrient iron absorption.

The overall conclusion of our study is that the LMM iron species detected in blood plasma are not the sought-after NTBI species. So what are these LMM species and where is NTBI? HPN is absent in macrophages[64] so Fe^{II} from these cells may be released into the blood and oxidized to Fe^{III} by CPN. We suggest that the LMM iron species that we observe are these Fe^{II}/Fe^{III} species. This explains why the detected LMM iron species are not associated directly with nutrient absorption; rather they may be more closely related to red blood cell recycling processes involving the macrophage release of iron and subsequent oxidation by CPN. These species may also arise from the iron exported by erythroid cells.[42] As far as the elusive NTBI, two possibilities seem reasonable. The first is that the NTBI in our plasma samples was/were adsorbed by our chromatography columns, and thus was/were not observed in our chromatograms. The second is that NTBI only appears in the plasma when TFN saturation is $>60\%$. We are investigating both possibilities.

Authors' contribution

JH performed the animal surgeries, animal husbandry, and pig blood withdrawals. ND organized the experiments, collected blood samples, prepared plasma, performed the LC-ICP-MS experiments, and helped analyzed the data. PAL conceived of the experiments, helped analyze the data, and wrote most of the paper. All authors edited the paper and agreed to its submission.

Abbreviations

CAV	Caudal vena cava
CRV	Cranial vena cava
CPN	Ceruloplasmin
FPN	Ferroportin
FTS	Flow-through solution
HMM	High molecular mass
HPN	Hephaestin
LC	Liquid chromatography
ICP-MS	Inductively coupled plasma mass spectrometry
NTBI	Nontransferrin bound iron
LMM	Low molecular mass
P1, P2, P3, and P4	Pigs 1–4 respectively
PV	Portal vein
TAMU	Texas A&M University
TFN	Transferrin
TIBC	Total iron binding capacity
VAP	Venous access port

Conflicts of interest

There are no conflicts to declare.

Acknowledgements

This work was supported by the National Institutes of Health (R35 GM127021), Texas A&M University College of Veterinary Medicine (RGS 16-04) and the Robert A. Welch Foundation (A1170-20190330). The content is solely the responsibility of the authors and does not necessarily represent the official views of the National Institutes of Health, Texas A&M University, or the Welch Foundation.

Notes and references

1 T. Ganz, Systemic iron homeostasis, *Physiol. Rev.*, 2013, **93**, 1721–1741.
2 S. Gulec, G. J. Anderson and J. F. Collins, Mechanistic and regulatory aspects of intestinal iron absorption, *Am. J. Physiol.: Gastrointest. Liver Physiol.*, 2014, **307**, G397–G409.
3 H. Drakesmith, E. Nemeth and T. Ganz, Ironing out Ferroportin, *Cell Metab.*, 2015, **22**, 777–787.
4 B. K. Fuqua, Y. Lu, D. Darshan, D. M. Frazer, S. J. Wilkins, N. Wolkow, A. G. Bell, J. Hsu, C. C. Yu, H. Chen, J. L. Dunaief, G. J. Anderson and C. D. Vulpe, The multicopper ferroxidase Hephaestin enhances intestinal iron absorption in mice, *PLoS One*, 2014, **9**, e98792.
5 A. Pietrangelo, Hereditary Hemochromatosis: pathogenesis, diagnosis, and treatment, *Gastroenterology*, 2010, **139**, 393–408.
6 A. C. G. Chua, J. K. Olynyk, P. J. Leedman and D. Trinder, Nontransferrin-bound iron uptake by hepatocytes is increased in the Hfe knockout mouse model of hereditary hemochromatosis, *Blood*, 2004, **104**, 1519–1525.
7 P. Brissot, M. Ropert, C. Le Lan and O. Loreal, Non-transferrin bound iron: a key role in iron overload and iron toxicity, *Biochim. Biophys. Acta*, 2012, **1820**, 403–410.
8 W. Breuer, C. Hershko and Z. I. Cabantchik, The importance of non-transferrin bound iron in disorders of iron metabolism, *Transfus. Sci.*, 2000, **23**, 185–192.
9 M. Grootveld, J. D. Bell, B. Halliwell, O. I. Aruoma, A. Bomford and P. J. Sadler, Non-transferrin-bound iron in plasma or serum from patients with idiopathic hemochromatosis – characterization by high-performance liquid chromatography and nuclear

magnetic resonance Chem spectroscopy, *J. Biol. Chem.*, 1989, **264**, 4417–4422.

10 L.-C. Konigsberger, E. Konigsberger, P. M. May and G. T. Hefter, Complexation of iron(III) and iron(II) by citrate. Implications for iron speciation in blood plasma, *J. Inorg. Biochem.*, 2000, **78**, 175–184.

11 P. M. May, P. W. Linder and D. R. Williams, Computer simulation of metal ion equilibria in biofluids: models for the low-molecular-weight complex distribution of calcium(II), magnesium(II), manganese(II), iron(III), copper(II), zinc(II) and lead(II) ions in human blood plasma, *J. Chem. Soc., Dalton Trans.*, 1977, **6**, 588–595.

12 L. de Swart, J. C. Hendriks, L. N. van der Vorm, Z. I. Cabantchik, P. J. Evans, E. A. Hod, G. M. Brittenham, Y. Furman, B. Wojczyk, M. C. Janssen, J. B. Porter, V. E. Mattijssen, B. J. Biemond, M. A. MacKenzie, R. Origa, R. Galanello, R. C. Hider and D. W. Swinkels, Second international round robin for the quantification of serum non-transferrin bound iron and liable plasma iron in patients with iron-overload disorders, *Haematologica*, 2016, **10**, 38–45.

13 E. Tolosano, S. Fagoonee, N. Morello, F. Vinchi and V. Fiorito, Heme scavenging and the other facets of hemopexin, *Antioxid. Redox Signaling*, 2010, **12**, 305–320.

14 D. Chiabrando, F. Vinchi, V. Fiorito, S. Mercurio and E. Tolosano, Heme in pathophysiology: a matter of scavenging, metabolism and trafficking across cell membranes, *Front. Pharmacol.*, 2014, **5**, 61.

15 I. Yanatori, M. Tabuchi, Y. Kawai, Y. Yasui, R. Akaji and F. Kishi, Heme and non-heme iron transporters in non-polarized and polarized cells, *BMC Cell Biol.*, 2010, **11**, 39–50.

16 D. J. Schaer, F. Vinchi, G. Ingoglia, E. Tolosano and P. W. Buehler, Haptoglobin, hemopexin, and related defense pathways—basic science, clinical perspectives, and drug development, *Front. Physiol.*, 2014, **5**, 415.

17 T. Peters, *All about albumin biochemistry, genetics and medical applications*, Academic Press, 1996.

18 R. A. Lovstad, Interaction of serum albumin with the Fe(III)–citrate complex, *Int. J. Biochem.*, 1993, **25**, 1015–1017.

19 R. W. Evans, R. Rafique, A. Zarea, C. Rapisarda, R. Cammack, P. J. Evans, J. B. Porter and R. C. Hider, Nature of non-transferrin-bound iron: studies on iron citrate complexes and thalassemic sera, *J. Biol. Inorg. Chem.*, 2008, **13**, 57–74.

20 M. Fasano, S. Curry, E. Terreno, M. Galliano, G. Fanali, P. Narciso, S. Notari and P. Ascenzi, The extraordinary ligand binding properties of human serum albumin, *IUBMB Life*, 2005, **57**, 787–796.

21 S. Recalcati, P. Invernizzi, P. Arosio and G. Cairo, New functions for an iron storage protein: the role of ferritin in immunity and autoimmunity, *J. Autoimmun.*, 2008, **30**, 84–89.

22 S. G. Gehrke, H. Kulaksiz, T. Herrmann, H. D. Riedel, K. Bents, C. Veltkamp and W. Stremmel, Expression of hepcidin in hereditary hemochromatosis: evidence for a regulation in response to the serum transferrin saturation and to non – transferrin-bound iron, *Blood*, 2010, **116**, 1574–1584.

23 L. A. Cohen, L. Gutierrez, A. Weiss, Y. Leichtmann-Bardoogo, D. L. Zhang, D. R. Crooks, R. Sougrat, A. Morgenstern, B. Galy, M. W. Hentze, F. J. Lazaro, T. A. Rouault and E. G. Meyron-Holtz, Serum ferritin is derived primarily from macrophages through a nonclassical secretory pathway, *Blood*, 2010, **116**, 1574–1584.

24 P. Arosio, M. Yokota and J. W. Drysdale, Characterization of serum ferritin in iron overload: possible identity to natural apoferritin, *Br. J. Haematol.*, 1977, **36**, 199–207.

25 S. Recalcati, P. Invernizzi, P. Arosio and G. Cairo, New functions for an iron storage protein: the role of ferritin in immunity and autoimmunity, *J. Autoimmun.*, 2008, **30**, 84–89.

26 W. Wang, M. A. Knovich, L. G. Coffman, F. M. Torti and S. V. Torti, Serum ferritin: past, present and future, *Biochim. Biophys. Acta*, 2010, **1800**, 760–769.

27 P. Brissot, T. L. Wright, W. L. Ma and R. A. Weisiger, Efficient clearance of non-transferrin-bound iron by rat liver: implications for hepatic iron loading in iron overload states, *J. Clin. Invest.*, 1985, **76**, 1463–1470.

28 J. J. Pinilla-Tenas, B. K. Sparkman, A. Shawki, A. C. Illing, C. J. Mitchell, N. N. Zhao, J. P. Liuzzi, R. J. Cousins, M. D. Knutson and B. Mackenzie, Zip14 is a complex broad-scope metal-ion transporter whose functional properties support roles in the cellular uptake of zinc and nontransferrin-bound iron, *Am. J. Physiol.: Cell Physiol.*, 2011, **301**, C862–C871.

29 J. P. Liuzzi, F. Aydemir, H. Ham, M. D. Knutson and R. J. Cousins, Zip14 (Slc39a14) mediates non-transferrin-bound iron uptake into cells, *Proc. Natl. Acad. Sci. U. S. A.*, 2006, **103**, 13612–13617.

30 J. M. C. Gutteridge, D. A. Rowley, E. Griffiths and B. Halliwell, Low-molecular-weight iron complexes and oxygen radical reactions in idiopathic haemochromatosis, *Clin. Sci.*, 1985, **68**, 463–467.

31 F. W. Huang, J. L. Pinkus, G. S. Pinkus, M. D. Fleming and N. C. Andrews, A mouse model of juvenile hemochromatosis, *J. Clin. Invest.*, 2005, **115**, 2187–2191.

32 B. P. Esposito, W. Breuer, P. Sirankapracha, P. Pootrakul, C. Hershko and Z. I. Cabantchik, Labile plasma iron in iron overload: redox activity and susceptibility to chelation, *Blood*, 2003, **102**, 2670–2677.

33 B. Sarkar, State of iron(III) in normal human serum – low molecular weight and protein ligands besides transferrin, *Can. J. Biochem.*, 1970, **48**, 1339–1350.

34 R. E. Fleming, M. C. Migas, X. Y. Zhou, R. S. Britton, E. M. Brunt, S. Tomatsu, A. Waheed, B. R. Bacon and W. S. Sly, Mechanism of increased iron absorption in murine model of hereditary hemochromatosis: increased duodenal expression of the iron transporter DMT1, *Proc. Natl. Acad. Sci. U. S. A.*, 1999, **96**, 3143–3148.

35 O. Loreal, I. Gosriwatana, D. Guyader, J. Porter, P. Brissot and R. C. Hider, Determination of non-transferrin-bound iron in genetic hemochromatosis using a new HPLC-based method, *J. Hepatol.*, 2000, **32**, 727–733.

36 I. Gosriwatana, O. Loreal, S. Lu, P. Brissot, J. Porter and R. C. Hider, Quantification of non-transferrin-bound iron in the presence of unsaturated transferrin, *Anal. Biochem.*, 1999, **273**, 212–220.

37 J. B. Porter, R. D. Abeysinghe, L. Marshall, R. C. Hider and S. Singh, Kinetics of Removal and Reappearance of Non – Transferrin-Bound Plasma Iron with Deferoxamine Therapy, *Blood*, 1996, **88**, 705–713.
38 N. Dziuba, J. Hardy and P. A. Lindahl, Low-molecular-mass iron in healthy blood plasma is not predominately ferric citrate, *Metallomics*, 2018, **10**, 802–817.
39 M. M. Swindle, Cardiothoracic and Vascular Surgery/ Chronic Intravascular Catheterization, *Swine in the laboratory. Surgery, anesthesia, imaging and experimental techniques*, CRC Press, Taylor & Francis Group, Boca Raton, FL, 2nd edn, 2007, vol. 9, pp. 195–259.
40 E. Landberg, E. Aström, B. Kagedal and P. Pahlsson, Disialotrisialo bridging of transferrin is due to increased branching and fucosylation of the carbohydrate moiety, *Clin. Chim. Acta*, 2012, **414**, 58–64.
41 M. Gudowska, E. Gruszewska, A. Panasiuk, B. Cylwik, M. Swiderska, R. Filisiak, M. Szmitkowski and L. Chrostek, Changed profile of serum transferrin isoforms in liver diseases, *Clin. Lab.*, 2017, **63**, 349–354.
42 N. D. Sharma, R. W. Evans and K. J. Patel, *et al.*, Evidence for the glycosylation of porcine serum transferrin at a single site located within the C-terminal lobe, *Biochim. Biophys. Acta, Protein Struct. Mol. Enzymol.*, 1994, **1206**, 286–288.
43 I. Graham and J. Williams, A comparison of glycopeptides from the transferrins of several species, *Biochem. J.*, 1975, **145**, 263–279.
44 M. Nagae, K. Morita-Matsumoto and S. Arai, *et al.*, Structural change of *N*-glycan exposes hydrophobic surface of human transferrin, *Glycobiology*, 2014, **24**, 693–702.
45 A. Helander and N. K. Modén, Effect of transferrin glycation on the use of carbohydrate-deficient transferrin as an alcohol biomarker, *Alcohol Alcohol.*, 2013, **48**, 478–482.
46 A. Van Campenhout, C. Van Campenhout, A. R. Lagrou and B. Manuel-Y-Keenoy, Effects of in vitro glycation on Fe^{3+} binding and Fe^{3+} isoforms of transferrin, *Clin. Chem.*, 2004, **50**, 1640–1649.
47 M. A. Siimes and P. R. Dallman, New Kinetic Role for Serum Ferritin in Iron Metabolism, *Br. J. Haematol.*, 1974, **28**, 7–18.
48 J. W. Halliday, U. Mack and L. W. Powell, The Kinetics of Serum and Tissue Ferritins: Relation to Carbohydrate Content, *Br. J. Haematol.*, 1979, **42**, 535–546.
49 M. N. Garcia-Casal, S.-R. Pasricha, R. X. Martinez, L. Lopez-Perez and J. P. Peña-Rosas, Serum or plasma ferritin concentration as an index of iron deficiency and overload, *Cochrane Database Syst. Rev.*, 2015, **7**, CD011817.
50 H. Drakesmith, E. Nemeth and T. Ganz, Ironing out ferroportin, *Cell Metab.*, 2015, **22**, 777–787.
51 S. Y. Jeong and S. David, Glycosylphosphatidylinositol-anchored ceruloplasmin is required for iron efflux from cells in the central nervous system, *J. Biol. Chem.*, 2003, **278**, 27144–27148.
52 K. Y. Yeh, M. Yeh, L. Mims and J. Glass, Iron feeding induces ferroportin I and hephaestin migration and interaction in rat duodenal epithelium, *Am. J. Phyisol. Gastrointest. Liver Physiol.*, 2009, **296**, G55–G65.
53 C. J. Mitchell, A. Shawki, T. Ganz, E. Nemeth and B. Mackenzie, Functional properties of human ferroportin, a cellular iron exporter reactive also with cobalt and zinc, *Am. J. Physiol.: Cell Physiol.*, 2014, **306**, C450–C459.
54 R. Taniguchi, H. E. Kato, J. Font, C. N. Deshpande, M. Wada, K. Ito, R. Ishitani, M. Jormakka and O. Nureki, Outward- and inward-facing structures of a putative bacterial transition-metal transporter with homology to ferroportin, *Nat. Commun.*, 2015, 8545, DOI: 10.1038/ncomms9545.
55 C. J. Mitchell, A. Shawki, T. Ganz, E. Nemeth and B. Mackenzie, Functional properties of human ferroportin, a cellular iron exporter reactive also with cobalt and zinc, *Am. J. Physiol.: Cell Physiol.*, 2014, **306**, C450–C459.
56 A. Donovan, Y. Brownlie, J. Zhou, S. J. Shepard, J. Pratt, B. H. Moynihan, A. Paw, B. Drejer, A. Barut, L. T. C. Zapata, C. Brugnara, S. E. Lux, G. S. Pinkus, J. L. Pinkus, P. D. Kingsley, J. Palls, M. D. Fleming, N. C. Andrews and I. Z. Leonard, Positional cloning of zebrafish ferroportin1 identifies a conserved vertebrate iron exporter, *Nature*, 2000, **403**, 776–781.
57 I. DeDomenico, D. M. Ward, M. C. B. di Patti, S. Y. Jeong, S. David, G. Musci and J. Kaplan, Ferroxidase activity is required for the stability of cell surface ferroportin in cells expressing GPI-ceruloplasmin, *EMBO J.*, 2007, **26**, 2823–2831.
58 A. T. McKie, P. Marciani, A. Rolfs, K. Brennan, K. Wehr, D. Barrow, S. Miret, A. Bomford, T. J. Peters, F. Farzaneh, M. A. Hediger, M. W. Hentze and R. J. Simpson, A novel duodenal iron-regulated transporter, IREG1, implicated in the basolateral transfer of iron to the circulation, *Mol. Cell*, 2000, **2000**(5), 299–309.
59 R. T. Zijlstra, R. Jha, A. D. Woodward, J. Fouhse and T. A. T. G. van Kempen, Starch and fiber properties affect their kinetics of digestion and thereby digestive physiology in pigs, *J. Anim. Sci.*, 2012, **90**, 49–58.
60 S. Hooda, J. J. Matte, C. W. Wilkinson and R. T. Zijlstra, Technical note: An improved surgical model for the long-term studies of kinetics and quantification of nutrient absorption in swine, *J. Anim. Sci.*, 2009, **87**, 2013–2019.
61 B. U. Metzler-Zebeli, M. G. Ganzie, R. Mosenthin and R. T. Zijlstra, Oat beta-glucan and dietary calcium and phosphorus differentially modify intestinal expression of proinflammatory cytokines and monocarboxylate transporter 1 and Cecal morphology in weaned pigs, *J. Nutr.*, 2012, **142**, 668–674.
62 S. P. McCormick, M. J. Moore and P. A. Lindahl, Detection of labile low-molecular-mass transition metal complexes in mitochondria, *Biochemistry*, 2015, **54**, 3442–3453.
63 M. Wojdyr, Fityk: a general purpose peak fitting program, *J. Appl. Crystallogr.*, 2010, **43**, 1126–1128.
64 J. Gitschier, C. D. Vulpe and Y.-M. Kuo, *et al.*, Hephaestin, a ceruloplasmin homologue implicated in intestinal iron transport, is defective in the sla mouse, *Nat. Genet.*, 1999, **21**, 195–199.